

Segmentation of Thin Structures in Volumetric Medical Images ¹

Michal Holtzman-Gazit, Ron Kimmel, Nathan Peled, Dorith Goldsher

Abstract—We present a new segmentation method for extracting thin structures embedded in 3D medical images based on modern variational principles. We demonstrate the importance of the edge alignment and homogeneity terms in the segmentation of blood vessels and vascular trees. For that goal the Chan-Vese minimal variance method is combined with the boundary alignment, and the geodesic active surface models. An efficient numerical scheme is proposed. In order to simultaneously detect a number of different objects in the image, a hierarchical approach is applied.

Index Terms—image segmentation, active contours, deformable models, energy minimization, level sets, variational principle

I. INTRODUCTION

MEDICAL ‘volumetric images’ are 3D images that contain several anatomical structures. These structures are analyzed by trained personnel - radiologists. Two different modes are applied in order to allow accurate interpretation and planning of diagnostic and therapeutic interventional procedures: 1) Analysis of a single object while ignoring its surrounding. 2) Analysis of an object as part of the whole picture, while keeping the surrounding visible.

In this paper we deal with blood vessels captured by computerized tomography (CT), a procedure known as ‘CT angiography’ (CTA). CTA imaging is performed using a radio-opaque contrast material, injected intravenously. This procedure significantly increases the density of the blood within the vessels compared to the surrounding tissues, thereby increasing the contrast between the two. Intracranial blood vessels are a special challenge, due to their anatomy and anatomical relations: They enter the skull, through foramens located in its

base, tapering distally within the skull, as crowded and, at times, tortuous, multiple threadlike elements.

The CTA images are produced when an organ is scanned at different layers and then the resulting two-dimensional slices are successively stacked one on top of the other. When viewed separately, one slice at a time, one dimension is ‘lost’. Exploring the planar slices, radiologists may find it difficult to interpret the geometry of the organ. A simple procedure that tries to capture the geometric structure in a single image is MIP (Maximal Intensity Projection). In this approach, the projection value is given by the maximal pixel intensity along the projection line. However, using MIP, thin vessels may be occluded by highly saturated bones.

Our goal is to automatically extract the blood vessels contained in volumetric images, and enable radiologists to view vascular trees as separate 3D objects. Bones are also extracted, allowing visualization of the interaction between bones and vessels. Traditional threshold methods [23] often fail in segmenting two adjacent objects with similar gray values. In this paper we couple variational measures that allow us to overcome some of these problems.

One of the main difficulties encountered in analyzing CTA images is that both bones and blood vessels appear with similar density compared to brain parenchyma. In other words, they both have similar gray values. When thresholding an image that includes both enhanced blood vessels and dense bones, they might be extracted as a single object. We thus apply a hierarchical segmentation method using variational tools that enable us to accurately extract bones and blood vessels as two separate 3D objects.

II. PREVIOUS WORK

In this section we review previous segmentation methods and focus on deformable models. In 2D, a simple curve defines the object boundaries. A given initial curve can evolve according to its geometry and the information in the image. The evolution is a result of minimizing an energy functional – a cost function – which is influenced

Michal Holtzman Gazit is with the Electrical Engineering Department, Technion - Israel Institute of Technology, Haifa 32000, Israel. (e-mail: mikih@tx.technion.ac.il)

Ron Kimmel is with the Computer Science Department, Technion - Israel Institute of Technology, Haifa 32000, Israel.

Nathan Peled is with Carmel Medical Center, Haifa, Israel.

Dorith Goldsher is with the Faculty of Medicine, Technion - Israel Institute of Technology and Rambam Medical Center, Haifa, Israel.

by image information along the curve and the intrinsic geometry of the curve. Minimization of such a measure leads to a curve that should coincide with the boundary of the object. The first variation of the functional is used to evolve a given curve towards a significant local minimum of the functional, by applying a gradient descent flow.

The first deformable model for image segmentation, known as the ‘snakes’ model was introduced in [27]. This deformable contour minimizes an energy functional along a curve, which is influenced by ‘internal’ and ‘external’ terms. The internal term controls the smoothness and linear elasticity of the curve, while the external part directs the curve to the locations of high image gradients.

The model is simple and linear, yet, the linearity of the ‘snake’ model causes different parameterizations of the same initial curve to converge to different minimizers. That is, the same initial trajectory may end up at different final trajectories. This undesired property is the outcome of the fact that the snake model minimizes a non-geometric measure.

In order to overcome these difficulties, Casseles et al. [5] and Malladi et al. [38] introduced a curve evolution equation based on geometric quantities. They propagated a curve subject to image-based forces coupled with geometric smoothing forces. The curve evolution is formulated by the Osher-Sethian level set method [46], in order to handle topological changes of the curve and overcome numerical difficulties. The basic flow includes a constant inflation force, coupled with geometric forces such as the curvature vector.

Later, the geodesic active contour model was proposed by Casseles et al. in [7] as a geometric-variational alternative for ‘snakes’. The idea, similar to the ‘snake’ model, is a minimization of a functional that integrates over an edge indicator function along a contour. However, the arbitrary parametrization in the ‘snake’ is replaced with the curve’s arclength. The edge indicator function obtains low values in image locations where the gradient is high. The geometric energy functional is given by,

$$E_{GAC} = \int g(C(s))ds,$$

where C is the evolving curve, g is the edge indicator function and s is the Euclidean arc length. Specifically, $g(x, y) : \mathbb{R}^2 \mapsto \mathbb{R}^+$ is an inverse edge indicator that yields low values near edges (high image gradient magnitude) and high values elsewhere. The first variation used as a curve evolution gradient descent process is given by

$$C_t = (\kappa g - \langle \nabla g, \vec{n} \rangle) \vec{n},$$

where κ is the Euclidean curvature and \vec{n} is the unit normal to the curve. It is also implemented via the level set framework that restricts the processing to a regular grid and allows numerical stability. In order to prevent the curve from shrinking to a point, a constant velocity term that penalizes small area can be added. This constant term was first introduced by Cohen in [13] as the ‘balloon force’. The geodesic active contour method was extended to handle surfaces in 3D in [6] and was accelerated by Goldenberg et al. [22], [21] by coupling with a narrow band approach [11], and an efficient numerical scheme called AOS [36], [37], [54] for cortex segmentation.

Apparently, the gradient magnitude edge indicator was not enough for capturing thin structures. The additional important information that was so far neglected was the orientation of the image gradients. In [53] Vasilevskiy and Siddiqi used maximization of the inner product between a vector field and the surface normal in order to construct an evolution that is used for segmentation of thin structures. If this vector field is the image gradient, the maximization yields a flow according to the Laplacian of the image in the direction of the normal, as shown by Kimmel and Bruckstein in [30]. This term is a reliable edge indicator for relatively low noise levels. In the case of high noise levels, additional regularization techniques are required.

At the other end, Chan and Vese in [8], [9], used integral region descriptors in their ‘active contours without edges’ model, which is a minimal variance criterion for cortex segmentation. Their model is a simplified version of the Mumford-Shah [44] piecewise constant model, which limits the number of regions. As before, it evolves a contour in the image plane, or a surface in volumetric data in order to detect objects with relatively similar intensity levels in the image. A related approach is [45] where a 3D directional edge term is coupled with a smoothing term in order to segment a single object from multiple non-uniform volume data sets.

Here, we integrate the better qualities of the above geometric methods in order to segment thin structures in volumetric medical images. We combine the Chan-Vese minimal variance model with a geometric edge alignment measure and the geodesic active surface model. Then, for the implementation we apply an efficient numerical scheme based on [21], [28], [54]. Finally, we explore a hierarchical approach that allows us to efficiently detect numerous objects in the image.

A. Other Thin Structure Segmentation Methods

Lorigo et al. [35] used codimension-two geodesic active contours for segmentation of tubular structures according to the theory developed in [2]. Their approach allows the flow of a geodesic active curve in 3D. It evolves a curve as a thin tube of ϵ -radius around it. This idea was implemented for segmentation of blood vessels in MRA (Magnetic Resonance Angiography) images.

In [16] Deschamps and Cohen introduced a method based on the Zhu-Yuille region competition model [55]. They used a functional that combines an integral over region descriptor measures and the geodesic active contour functional [7].

Following Cohen and Kimmel [14], Deschamps and Cohen [17] presented a segmentation method based on Sethian's fast marching method [50], see [52] for a related fast Eikonal solver. Given a potential field g with lower values near the edges, the fast marching method is designed to find an image-dependant distance from a seed point that is located at the root of the anatomic tree structure. The equivalence between this measure and the geodesic active contour was shown in [14], [29]. The motion of a propagating weighted distance wave at points that are located along the boundary is slower compared to the rest of the propagating front, and for better stability, these points were virtually 'frozen' in [17].

In [42] McInerney and Terzopoulos used topology adaptive deformable snakes, T-snakes, for segmentation of medical images. The T-snake is a discrete form of a parametric deformable curve that moves according to the influence of internal and external forces. The grid points inside the curve are assumed to be 'on' (positive) and the points outside the curve are assumed to be 'off' (negative). As the curve moves, once a grid point is turned 'on', it cannot be turned 'off' again. The snake is periodically re-parameterized in order to maintain numerical stability. This method was extended to 3D (T-surface) in [43]. It is an interesting combination of the level set concept for preserving the topology by a regular supporting grid and a non-geometric parametric model.

In [33] Leventon et al. used a probabilistic approach in order to introduce shape information into the image segmentation process. In order to build a shape model, each curve is represented using a signed distance map. Then, a shape model is generated by defining a probability density function over the variances of a set of training shapes. In each step of the curve evolution, the shape and pose parameters of the final curve are estimated using a maximum a posteriori approach. The evolution of the curve is computed as a weighted sum of a 'shape force'

and the geodesic active contour force.

B. Recent Medical Images Segmentation Techniques

Recent segmentation techniques for thin structures include [18], where 'medial atoms' are used to segment branching tubular structures, a user-defined B-spline template snakes that initialize a segmentation process [41], and active shape model for segmenting abdominal aortic aneurysms, where a set of landmark points that denote the same anatomical points are matched [15]. Often, similar to [21], [22], several resolution levels enable more efficient coarse to fine fitting.

When the fully automatic model fails, interactive models are used. Such an approach was introduced by Paragios [47] who added user constrained active contour coupled with shape priors.

Local pattern matching was used in [19] in order to segment brain tumors from MR images. High order Gibbs prior model was coupled by Chen et al. [10] with Marching Cubes to initialize a deformable model.

Hernandez et al. [26], used the geodesic active contour model with non-parametric statistical information, to segment aneurysms in brain CTA images. As in [16], the region descriptors are the logarithm of the probability model, yet in this case the distribution is not Gaussian. The method was applied to detect aneurysms in the Circle of Willis.

In [25], another histogram based statistical approach was used to segment blood vessels from MRA images. The vessels intensity is modelled by a normal distribution. The parameters of the distributions are modelled by the EM (Expectation Maximization) algorithm.

In the next section we present our segmentation technique. Its main advantage over most existing methods is its ability to automatically segment thin structures in volumetric data. We use a variational geometric model that integrates the nice properties of existing techniques with new ones. A useful term is our extension of the Haralick/Canny edge detector that we introduce in a variational setting. We present an efficient numerical scheme for fast convergence. In addition, we apply a hierarchical method in order to efficiently detect multiple different anatomical structures with similar relative intensities.

III. 3D IMAGE VARIATIONAL SEGMENTATION

Our method is based on geometric active surfaces that evolve according to geometric partial differential equations until they stop at the boundaries of the objects. We use a weighted sum of three integral measures, an alignment term that leads the evolving surface to the edges of the desired object, a minimal variance term that

measures the homogeneity inside and outside the object, and a geodesic active surface term that is used mainly for regularization. In the following sections we motivate each term of our functional.

A. Edge-Based Techniques in 2D

Zero crossings of the second order derivative along the gradient direction were introduced by Haralik [24] and then used by Canny [4] as 2D edge detectors. Haralik observed that using only the gradient direction component of the Laplacian yields better edges than those produced by the zero crossing of the Laplacian (known as the Marr-Hildreth [40] edge detector). Based on the ‘Haralik edge detector’, Kimmel and Bruckstein [31], [32] developed a new edge integration scheme. The curve evolves along the second order derivative in the direction of the image gradient.

Consider a gray level image $I(x, y) : \mathbb{R}^2 \rightarrow [0, 1]$, where I_x and I_y are the first order derivatives in the horizontal and vertical directions, respectively. We define the gradient direction vector field

$$\vec{\xi}(x, y) = \frac{\nabla I}{|\nabla I|} = \frac{\{I_x, I_y\}}{\sqrt{I_x^2 + I_y^2}}, \quad (1)$$

and the orthogonal vector field

$$\vec{\eta}(x, y) = \frac{\bar{\nabla} I}{|\nabla I|} = \frac{\{-I_y, I_x\}}{\sqrt{I_x^2 + I_y^2}}. \quad (2)$$

Hence $\langle \vec{\xi}, \vec{\eta} \rangle = 0$. The Haralik edge detector finds the image locations where both $|\nabla I|$ is greater than some threshold and $I_{\xi\xi} = 0$, where $I_{\xi\xi}$ is the second derivative of I in the gradient direction.

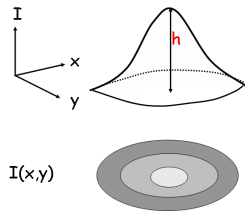


Fig. 1. The result of $\iint I_{\eta\eta} dx dy$ is $2\pi h$.

We would like to propagate an initial contour C that would stop as close as possible to our object’s boundaries. For that end, we use an energy functional – a cost function – which we derive using calculus of variations in order to find its extremum. Its derivative is an Euler-Lagrange (EL) equation that we use via the gradient descent flow in order to evolve our initial curve. Therefore, we need a geometric functional that would

yield $I_{\xi\xi}\vec{n} = 0$ as an EL (Euler-Lagrange) equation, where \vec{n} is the unit normal to the curve. In [31], [32] the authors use the fact that $I_{\xi\xi} = \Delta I - I_{\eta\eta}$ to show that the maximization of the functional,

$$\int_C \langle \nabla I, \vec{n} \rangle ds - \iint_{\Omega_C} \kappa_I |\nabla I| dx dy, \quad (3)$$

yields $I_{\xi\xi}\vec{n} = 0$ as the EL equation. Here, κ_I is the curvature of the level set of the image (equi-intensity contours or ‘isophotes’ in the image), and Ω_C is the area inside the curve C . We have that,

$$I_{\eta\eta} = \iint_{\Omega_C} \kappa_I |\nabla I| dx dy = \int_{\mathbb{R}^{I^{-1}(u)} \cap \Omega_C} \kappa_I ds du, \quad (4)$$

where s is a level set contour arclength and u represents the gray levels of the image. The integral $\int \kappa_I ds$ along a closed curve is 2π [32]. Therefore, the integral over $I_{\eta\eta}$ inside the curve measures the topological complexity of the image – the variability of gray levels – inside that curve. Thereby, the above functional maximizes the alignment between the image gradient and the edge normals while minimizing the topological complexity of the image inside the curve; see Figure 1.

Extension to 3D: Let us extend the scheme used in [31], [32] to 3D. In this case, the 3D image is defined as $I(x, y, z) : \mathbb{R} \rightarrow [0, 1]$. For this goal we first prove that,

$$I_{\xi\xi} = \Delta I - H_I |\nabla I|, \quad (5)$$

where H_I is the mean curvature of the level set surfaces of the volumetric image. In this case, the level sets are surfaces in the volumetric image data.

Lemma: The ‘Haralick-Canny-like’ edge detector in 3D is given by

$$I_{\xi\xi} = \Delta I - H_I |\nabla I|.$$

Proof:

$$\begin{aligned} I_{\xi\xi} &\equiv \langle \nabla \langle \nabla I, \xi \rangle, \xi \rangle = \langle \nabla (I_x \xi_1 + I_y \xi_2 + I_z \xi_3), \xi \rangle \\ &= I_{xx} \xi_1^2 + I_{xy} \xi_1 \xi_2 + I_{xz} \xi_1 \xi_3 + I_{yy} \xi_2^2 + I_{xy} \xi_1 \xi_2 \\ &\quad + I_{yz} \xi_2 \xi_3 + I_{zz} \xi_3^2 + I_{zy} \xi_3 \xi_2 + I_{xz} \xi_1 \xi_3 \\ &= \frac{I_x^2 I_{xx} + I_y^2 I_{yy} + I_z^2 I_{zz}}{|\nabla I|^2} \\ &\quad + \frac{2(I_x I_y I_{xy} + I_x I_z I_{xz} + I_y I_z I_{yz})}{|\nabla I|^2} \\ &= \Delta I - \operatorname{div} \left(\frac{\nabla I}{|\nabla I|} \right) |\nabla I| = \Delta I - H_I |\nabla I| \end{aligned}$$

■

The functional that yields $I_{\xi\xi}\vec{n} = 0$ as an EL equation in 3D has two parts:

1. Maximizing the geometric integral measure

$$\iint_S \langle \nabla I, \vec{n} \rangle da, \quad (6)$$

where S is the evolving surface, da is the surface area element and \vec{n} is the unit normal to the surface. The EL equations of this functional are

$$\Delta I \vec{n} = 0. \quad (7)$$

2. Minimizing the functional $\iiint_{\Omega_S} H_I |\nabla I| dx dy dz$, where Ω_S is the volume enclosed by the surface S . The EL equations are

$$H_I |\nabla I| \vec{n} = 0. \quad (8)$$

This functional is equal to

$$\int_{\mathbb{R}} \iint_{I^{-1}(u) \cap \Omega_S} H_I da du. \quad (9)$$

Here, da is the surface area element representing the image level sets, and $u = I(x, y, z)$ represents their gray values. This is a measure for uniformity inside the surface S .

Therefore, the energy functional that yields $I_{\xi\xi} \vec{n} = 0$, is given by

$$E_{\text{EDGE}}(S) = \iint_S \langle \nabla I, \vec{n} \rangle da - \iiint_{\Omega_S} H_I |\nabla I| dx dy dz. \quad (10)$$

This measure tracks edges of objects with low contrast compared to their background which is important for finding edges of thin structures in volumetric medical images. However, this term alone is insufficient for integrating all the edges. If the surface used as an initial guess is far from the object boundaries, it may fail to lock onto its edges. Therefore, another ‘force’ that pushes our surface toward the edges of the object is required.

B. Minimal Variance

The second measure we use is the minimal variance term proposed by Chan and Vese [8]. It penalizes lack of homogeneity inside and outside the evolving surface. In [8], the image is divided into two segments, the interior and exterior of a closed surface. This model minimizes the variance in each segment. The model was generalized in [9] to piecewise constant segmentation of more than two segments.

Given a 2D gray level image $I(x, y) : \Omega \rightarrow \mathbb{R}^+$, Chan and Vese proposed to use a minimal variance criterion given by the functional,

$$E_{\text{MV}}(C, c_1, c_2) = \iint_{\Omega_C} (I - c_1)^2 dx dy$$

$$+ \iint_{\Omega \setminus \Omega_C} (I - c_2)^2 dx dy + \nu \int_C ds, \quad (11)$$

where C is the contour separating the two regions, Ω_C is the interior of the contour $C = \partial\Omega_C$, and $\int_C ds$ measures the length of the separating contour, where ν is a constant that determines the regularization level. While minimizing this functional, c_1 and c_2 obtain the mean intensity values of the image in the interior and the exterior of C , respectively. The optimal curve would separate the interior and the exterior with respect to their relative expected values.

C. Geodesic Active Surface

Consider the functional $\iint_S da$, where da is a surface area element. This functional measures the surface area. Minimization of this functional yields an EL equation which defines a minimal surface for which the mean curvature is equal to zero. Hence, mean curvature flow is used for regularization in many schemes.

The geodesic active surface model [6], [7] is defined by the functional

$$E_{\text{GAC}}(S) = \iint g(S) da, \quad (12)$$

where da is the surface area element and $g(x, y, z)$ is again an edge indicator function, given, for example, by $g(x, y, z) = 1/(1 + |\frac{\nabla I}{\alpha}|^2)$.

The parameter α is used to normalize the gradient. It is chosen such that g gets close to zero along the edges of our object and higher values elsewhere. When minimizing this functional [7], the result is a surface along which g obtains the smallest possible values. The EL equation for this functional is $(gH - \langle \nabla g, \vec{n} \rangle) \vec{n} = 0$. Here, H is the mean curvature of the surface S , and \vec{n} is the normal to the surface. To learn more about the difference between this term and the edge alignment term, we refer the reader to [32], [29].

The regularization function that is used in our scheme is the geodesic active surface. Its added value over the area minimization via the mean curvature flow is its sensitivity to the actual data via the function g , which guides the evolving surface toward the desired object’s boundaries.

D. The Proposed Functional

The proposed functional is a weighted sum of the terms discussed in the previous subsections.

$$E_{\text{T}} = -E_{\text{EDGE}} + \beta E_{\text{MV}} + \gamma E_{\text{GAC}}, \quad (13)$$

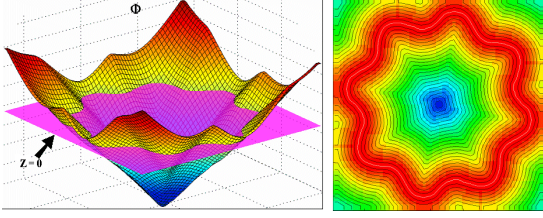


Fig. 2. Implicit representation of a curve given by a signed distance map. The curve is defined by the intersection of the plane $\{x, y, z = 0\}$ and function $\Phi(x, y)$.

where β, γ are positive constants that are chosen empirically. The geodesic active surface is used for regularization, thus γ is much smaller than β . These parameters were modified for different types of images (brain CTA, lung CT, MRI [Magnetic Resonance Imaging] etc.) but for a certain type of images we used the same set of parameters. Our rule of thumb for determining the best coefficients is that, when the image has a large amount of noise, β should be large, else it should be small. Moreover, when the variance of gray scales inside the object is large, β should be small.

The surface evolution toward an extremum derived from this functional is given by

$$S_t = \frac{\{-I_{\xi\xi} - \beta[(I - c_1)^2 - (I - c_2)^2] + \gamma(gH - \langle \nabla g, \vec{n} \rangle)\} \vec{n}}{|S_t|} \quad (14)$$

Our method integrates three ‘forces’: a Haralick alignment term that orients the evolving surface to align along the edges of the desired object, a homogeneity term based on the Chan-Vese functional, and a geodesic active surface term which is used for regularization. In the next section we discuss the numerical implementation using level set formulation and a semi-implicit scheme.

IV. NUMERICAL IMPLEMENTATION

A. Level Set Formulation

A curve can be represented by embedding it as an equal height contour of a certain function. This way the intersection between the function and, for example, the zero plane yields the curve. The curve is thereby represented implicitly by a higher dimensional function. We embed the curve C in as a function $\Phi(x, y)$ so that $C = \{\{x, y\} | \Phi(x, y) = 0\}$ is its zero level set. An example is shown in Figure 2. When curve evolution is written in terms of its implicit representation, a formulation known as the Osher-Sethian level set method [46]), the result is a stable numerical scheme that naturally handles topological changes. An example is given in Figure 3. Similarly in 3D, we embed a closed surface

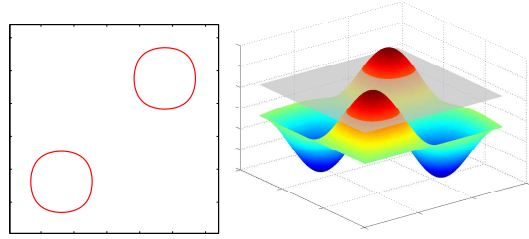


Fig. 3. Two simple curves (left) can be represented as a level set of a single function (right).

in a higher dimensional $\Phi(x, y, z)$ function, which implicitly represents the surface S as a zero level set, i.e. $S = \{\{x, y, z\} | \Phi(x, y, z) = 0\}$. According to the Osher-Sethian level set formulation [46], given a surface evolution $S_t = V_n \vec{n}$, its corresponding implicit level set evolution reads $\Phi_t = V_n |\nabla \Phi|$. The term V_n represents the ‘speed’ of the evolving surface in the direction of the normal to the surface. In our case,

$$V_n = \frac{-I_{\xi\xi} - \beta[(I - c_1)^2 - (I - c_2)^2] + \gamma(gH - \langle \nabla g, \vec{n} \rangle)}{|S_t|} \quad (15)$$

The level set formulation of our surface evolution equation is thereby

$$\Phi_t = \frac{\{-I_{\xi\xi} - \beta[(I - c_1)^2 - (I - c_2)^2] + \gamma \left[\text{div} \left(g \frac{\nabla \Phi}{|\nabla \Phi|} \right) \right]\} |\nabla \Phi|}{|\nabla \Phi|} \quad (16)$$

B. Numerical Scheme

We set $\Phi(x, y, z; t)$ to be a signed distance function of the surface $S(t)$ (positive values inside and negative values outside the surface). Since Φ is a distance map, we can write the *short time* evolution equation for which $|\nabla \Phi|$ is approximately equal to 1 near the zero level set surface, and we thereby simplify the short time evolution equation by replacing $|\nabla \Phi|$ with 1. Again, as our focus is the geometric behavior of the zero set surface rather than its implicit representation, this assumption does not violate the numerical consistency of the surface evolution PDE.

Nevertheless, the evolving surface may have singularities of its curvature. As those singularity sets are curves in 3D, the unit magnitude assumption is the best numerical approximation for $|\nabla \Phi|$ at the numerical grid points. An explicit up-wind scheme without re-initialization during the last iterations eliminates all minor inaccuracies and better fits the surface to the exact boundary location.

Re-initialization of Φ to a signed distance map can be done by a fast Eikonal solver [49], [52]. In order to

reduce the computational complexity we apply a narrow band approach [1], [11], [48]. Here, Φ has a volume similar to that of the original image. After each iteration we compute the distance only at grid points of Φ , that are close to the zero set. This way we have an efficient explicit scheme. However, explicit schemes are restricted by small time steps due to stability issues. The time step is a global parameter that determines the distance that the evolving surface is allowed to move at each iteration. Our explicit scheme is,

$$\Phi^{k+1} = \Phi^k + \tau(\gamma \operatorname{div}[g \nabla(\Phi^k)] + I_{\xi\xi} + \beta[(I - c_1)^2 - (I - c_2)^2]) \quad (17)$$

where τ is the time step, k is the iteration number, and Φ is initialized to be a distance function at each iteration.

In order to construct an unconditionally stable scheme we use a locally one-dimensional (LOD) scheme [39] suggested in [28]. The $\operatorname{div}(g \nabla(\Phi))$ operator can be written as a sum of matrix operators,

$$\operatorname{div}(g \nabla(\Phi)) = \frac{\partial}{\partial x} \left(g \frac{\partial}{\partial x} \Phi \right) + \frac{\partial}{\partial y} \left(g \frac{\partial}{\partial y} \Phi \right) + \frac{\partial}{\partial z} \left(g \frac{\partial}{\partial z} \Phi \right) = \sum_{l=x,y,z} A_l(\Phi). \quad (18)$$

Each A_l is a tri-diagonal matrix operator, which represents a one-dimensional operator given by $A_l = \frac{\partial}{\partial l} g \frac{\partial}{\partial l}$, where $l = x, y, z$. Next, we use the approximation

$$(1 - \tau A)^{-1} = 1 + \tau A + O(\tau^2) \approx 1 + \tau A. \quad (19)$$

Our first order numerical scheme reads as follows

$$\Phi^{k+1} = \prod_{l=1}^3 (\mathcal{I} - \tau \gamma A_l)^{-1} (\Phi^k + \tau f), \quad (20)$$

where, $f = -\{\beta[(I - c_1)^2 - (I - c_2)^2] + I_{\xi\xi}\}$. Here \mathcal{I} is the identity matrix. This allows us to successively solve three one-dimensional problems.

According to [54], a simple discretization for A_x is

$$\frac{\partial}{\partial x} g \frac{\partial}{\partial x} \Phi_i \approx \sum_{j \in N(i)} \frac{g_j + g_i}{2h_x^2} (\Phi_j - \Phi_i), \quad (21)$$

where $N(i)$ are indices of the two horizontal neighbors of pixel i : $\{i - 1, i + 1\}$, and h_x is the space between neighboring pixels. In order to invert these tri-diagonal matrices the Thomas algorithm [3] is used.

The LOD scheme [39] is an unconditionally stable scheme that allows a time step of any size. Let $B_l = \mathcal{I} - \tau \gamma A_l$. B_l is strictly diagonally dominant (i.e. $b_{ii}^l > 0$ and $b_{ij}^l < 0$ for $i \neq j$). Therefore, B_l^{-1} is nonnegative in all its arguments. In addition, the row sums of B_l are all 1. These attributes imply that the LOD scheme computes Φ^{n+1} from convex combinations of the elements of Φ^n .

Therefore, the discrete minimum-maximum principle is guaranteed

$$\min_j \Phi_j^n \leq \Phi_i^{n+1} \leq \max_j \Phi_j^n \quad \forall i, \quad (22)$$

and the scheme is stable in the maximum norm for any size of τ .

The LOD scheme is used in order to accelerate the propagation of the surface in a stable way. A large time step is used, and the scheme converges efficiently. For the final few iterations we apply an explicit scheme as a ‘final touch’ for better accuracy. For an image of size 100^3 voxels, the program runs a couple of minutes on a Pentium IV PC using double precision.

V. EXTRACTION OF MULTIPLE OBJECTS

In most cases, medical images contain a number of objects that need to be extracted in order to analyze an object and its environment. Here we propose a hierarchical approach for extracting multiple objects. The Chan-Vese multi-level set approach [9], uses several functions to form different binary codes that describe multiple regions. Each binary code tags a given region, and n different regions, require $\lg n$ functions. For better efficiency, here we first separate between similar looking objects and their background using a single function, and only then focus on segmenting between the objects themselves. This way we deal with one function at a time, and reduce the domain of the problem at each segmentation step.

A. Hierarchical Approach

In order to extract several different types of anatomical structures from the image, we use a hierarchical method that is conceptually similar to single node splitting in tree structured vector quantization (TSVQ) [20]. In TSVQ the image is quantized into 2^m regions by applying the following algorithm. First, the image is divided into two regions by using the generalized Lloyd algorithm [34]. Next, the data is split into two subsets, and a codebook of size two is generated using the generalized Lloyd algorithm on each subset. This process is repeated until level $m - 1$ is reached. At the end of this algorithm we have a tree of codewords (each word represents a region) in which the leaves form the final codebook.

A different method for finding the TSVQ is to use single node splitting [20]. This way, after the first quantization step, only one subset of the data is split into two new subsets. In each step, only one node in the tree is chosen for further splitting. One way of choosing the next segment to split, is by selecting the one that has the

greatest inhomogeneity. Our hierarchical segmentation method is designed in a similar way. At each stage we choose one subregion that includes more than one object, and split it into two subregions.

For a given image, we first apply the segmentation algorithm described in the previous sections. The result is a surface that describes the boundary of the segmented object. If there is a need for further segmentation, we apply our segmentation algorithm again, only to one of the regions generated from the previous step. This way, we can focus our segmentation algorithm on processing only the significant parts of the image. Moreover, since in the second step, the algorithm works only on part of the image, its computational complexity is significantly reduced.

A similar hierarchical approach was used in [51], where Tsai et al. used the piecewise smooth Mumford-Shah functional [44], for both smoothing and segmentation. Here, we use the hierarchical method with the alignment term, region homogeneity, and boundary regularity, which generalizes existing methods. Specifically, it enables us to handle the delicate task of thin structure segmentation in 3D.

VI. EXPERIMENTAL RESULTS

Next, we present the segmentation results of our algorithm using the hierarchical approach. Figure 5 shows a 3D hierarchical segmentation of CT angiography images of the brain. We applied the first step of our algorithm to part of the whole CTA volumetric image. The MIP (maximal intensity projection) of this image is shown in Figure 4 on the left and a 2D slice of this image is shown on the right. In this image the vessels appear in light gray while the bones appear in white. We initialized the surface as a small balloon inside one of the blood vessels and allowed it to grow toward the boundaries. In this experiment $\beta = 0.4$ and $\gamma = 0.01$. These coefficients were used for all our experiments with brain CTA images. The result of the first step of the segmentation is shown in Figure 5 left. See Figure 6 for another view. The algorithm captured the bright parts of the image, which include both the bones and the blood vessels. In order to distinguish between the two objects we applied the second step of the algorithm only to the region segmented during the first step. The results are shown in Figure 5 right.

Another example is an aneurysm in the brain. An aneurysm, especially when small, might be difficult to detect even by an expert looking at the 2D slices. However, when viewed as a geometric structure it can be seen clearly. Results are shown in Figure 7.

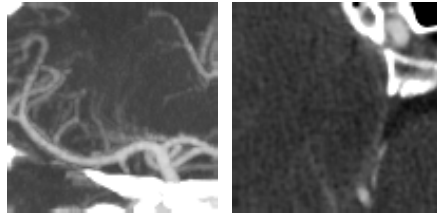


Fig. 4. Left: Maximal intensity projection (MIP) of a 100^3 volume of a CTA image of the brain. Right: A 100^2 part of a 2D CTA image of the brain. The bones adjacent to the brain appear in high density as white, and the blood vessels appear in lower density as light gray.

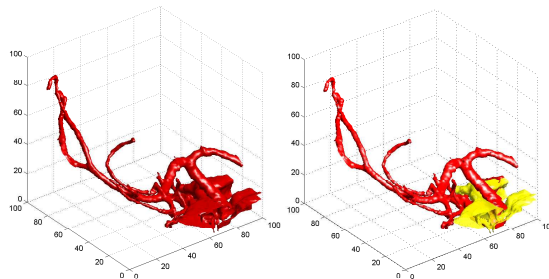


Fig. 5. Left: The result of the first phase of the segmentation algorithm on the CTA image. Right: Results of the hierarchical segmentation on the CTA image of the head. The yellow surface demonstrates the bone and the red surface represents the blood vessels.

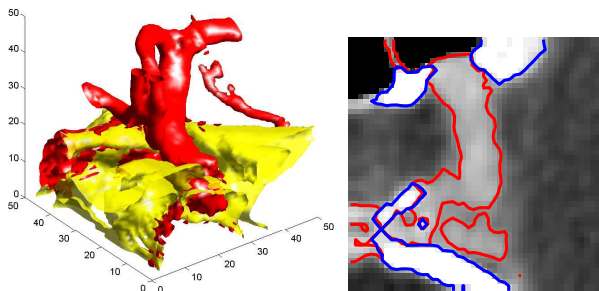


Fig. 6. Left: The hierarchical algorithm applied to a 3D CT image of the brain. The yellow surface depicts the bone data while the red surface depicts the vessels. Right: A 2D slice of the CT data of the brain showing the contours of the two objects generated by our segmentation algorithm.

When dealing with MRI of the brain, we have a similar problem of segmenting the gray matter and the white matter as two different objects. Figure 8 shows the segmentation result of the hierarchical segmentation for a 3D MRI image generated by the BrainWeb [12]. In this image we used $\beta = 0.5$ and $\gamma = 0.01$. Figure 8 also shows a perspective view of the gray and white matter generated by our segmentation algorithm.

We applied our algorithm to CT image of one of

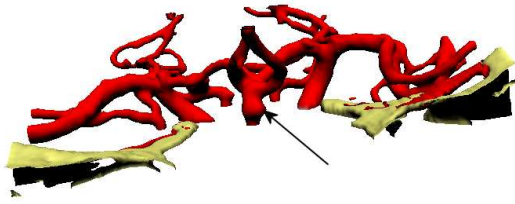


Fig. 7. The hierarchical segmentation result of a part of a CTA of the brain with an aneurysm. The aneurysm is pointed to with the arrow. The bones are depicted in yellow while the vessels appear in red.

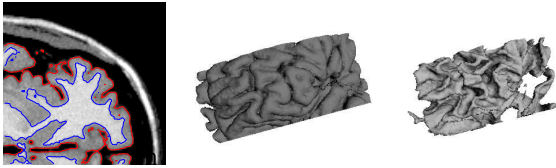


Fig. 8. Results of the hierarchical segmentation. Left: The result of the first phase is the red contour. The second phase yields the blue contour. Middle and right are gray and white matter surfaces respectively.

the saccular thoracic organs. In this image, as for the brain, it is important to track vessels with small caliber in order to determine if there are pathological lesions around them. In this case the alignment term is amplified in order to detect the edges of these fine vessels. The results of our algorithm with different weights on the alignment terms are shown in Figure 9. When comparing the segmented result of the minimal variance term alone (see Figure 9(c)) to the segmentation results using the minimal variance term together with the alignment term, we see that these fine vessels are detected when the alignment term has a larger influence (see Figures 9(a) and 9(b)). This variational measure is indeed helpful in finding the edges of thin structures with low contrast.

VII. CONCLUSIONS AND DISCUSSION

We presented a new segmentation method of 3D medical images. The method is based on a weighted sum of three integral measures that account for the minimal variance within each region, the alignment of the boundary with the change of intensity, and the weighted arclength for regularization. The importance of the new alignment term in the segmentation of thin structures in volumetric medical images was demonstrated. An efficient numerical scheme for the proposed method was introduced in order to accelerate its convergence. Next, an hierarchical approach was applied to efficiently segment several different anatomical structures with similar intensity values.

The numerical scheme accelerated the convergence of the segmentation. However, our system still does not work in real time. The bottleneck is the double precision calculations. In order to shorten the running time a fixed point strategy should be considered. There is still a need to examine the resolution of the fixed point for each part of the scheme in order to maintain its accuracy and convergence.

The functionals we dealt with are not convex. Therefore, gradient descent processes stop at local minima. One challenge is tracking down the significant minimum. This is realized, for example, by initializing the surface inside the object of interest, within the basin of attraction of the significant minimum, such as a small sphere at one of the main arteries in the brain. Nevertheless, there are obvious cases where the segmentation process fails to find the entire structure. In some cases the vessels are so thin (less than the sampling rate) and of low contrast, so that the evolving surface splits, leaving two parts of the same blood vessel as disconnected components. One remedy is to apply a topology preserving scheme, which tracks the topology of the surface. Yet, another option is to incorporate priors. Shape priors could be integrated and used for known structures such as bones. This way, the partition between blood vessels and bones could be improved in the second stage of our algorithm. However, prior based methods are somewhat dangerous in medical data analysis. Probably the most promising direction is user guided segmentation. Such a procedure would allow the user to interactively correct segmentation results of problematic regions where the fully automatic segmentation fails.

VIII. ACKNOWLEDGEMENTS

We thank Dr. Yoav Schechner from the Technion, for his help during the preparation of this manuscript. This research was partly supported by GIF – German Israeli Foundation grant number 615/99 and by the Ministry of Science Infrastructure grant number 01 – 01 – 01499.

REFERENCES

- [1] D. Adalsteinsson and J. Sethian, “A fast level set method for propagating interfaces,” *J. of Comp. Phys.*, vol. 118, pp. 269–277, 1995.
- [2] L. Ambrosio and H. Soner, “Level set approach to mean curvature flow in arbitrary codimension,” *J. of Diff. Geom.*, vol. 43, pp. 693–737, 1996.
- [3] W. Ames, *Numerical Methods for Partial Differential Equations*, 2nd ed. New York: Academic Press, 1977, p. 52.
- [4] J. Canny, “A computational approach to edge detection,” *IEEE Trans. Pattern Anal. Machine Intell.*, vol. 8(6), pp. 679–698, 1986.
- [5] V. Caselles, F. Catte, T. Coll, and F. Dibos, “A geometric model for active contours,” *Numerische Mathematic*, vol. 66, pp. 1–31, 1993.

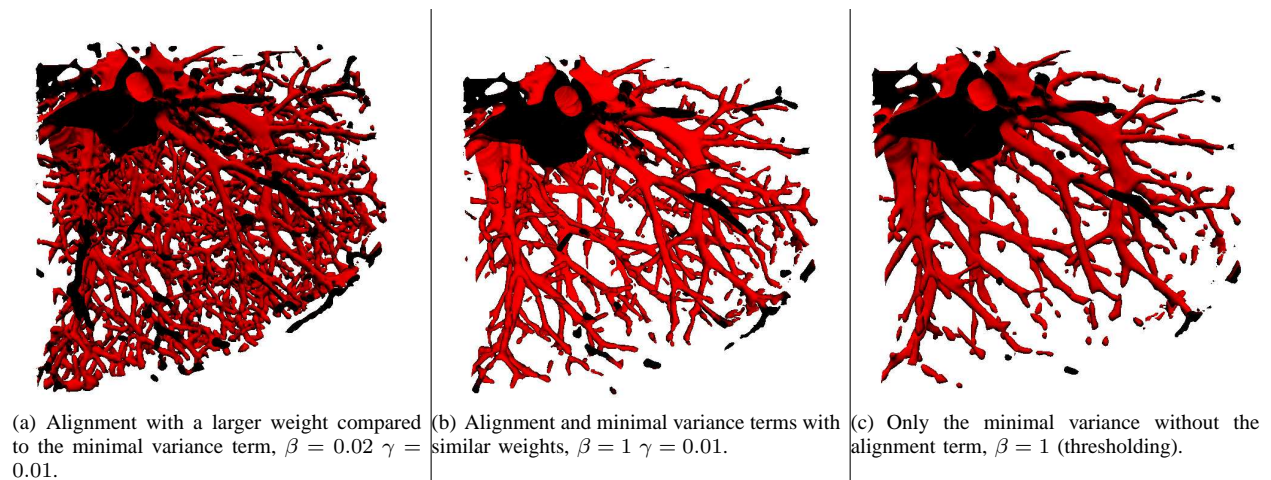


Fig. 9. Segmentation results of part of the thorax CT using different segmentation criteria.

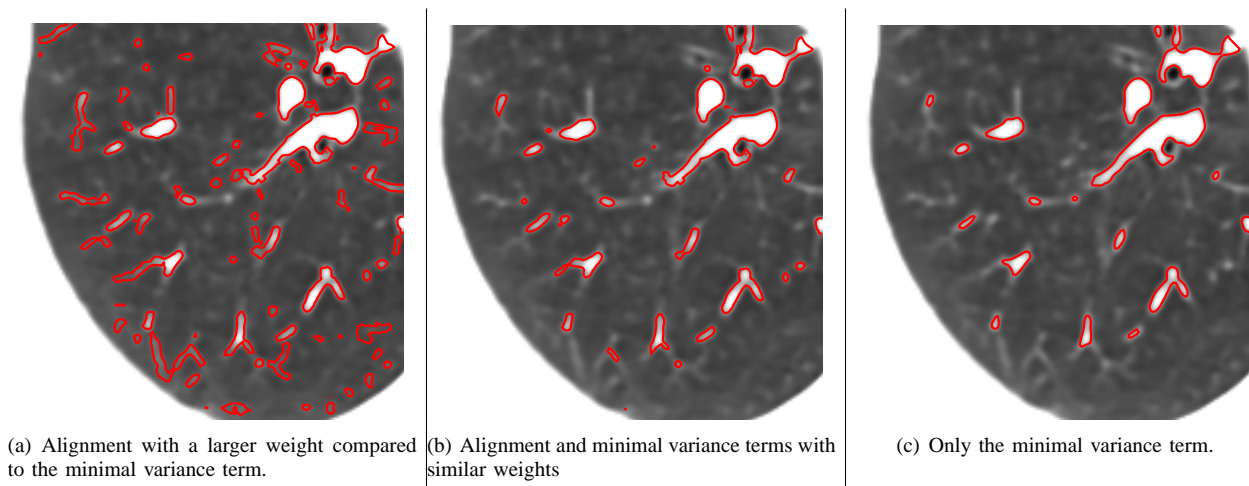


Fig. 10. Segmentation results of part of the thorax CT using different segmentation criteria. A 2D contour demonstrates the segmentation result painted on the original CT slice.

- [6] V. Caselles, R. Kimmel, G. Sapiro, and C. Sbert, "Minimal surfaces based object segmentation," *IEEE Trans. Pattern Anal. Machine Intell.*, vol. 19, no. 4, pp. 394–398, 1997.
- [7] V. Caselles, R. Kimmel, and G. Sapiro, "Geodesic active contours," *Int. Journal of Comp. Vis.*, vol. 22(1), pp. 61–79, 1997.
- [8] T. Chan and L. Vese, "Active contours without edges," *IEEE Trans. Image Processing*, vol. 10, no. 2, pp. 266–277, 2001.
- [9] —, "A multiphase level set framework for image segmentation using the Mumford and Shah model," *Int. Journal of Comp. Vis.*, vol. 50, no. 3, pp. 271–293, 2002.
- [10] T. Chen and D. Metaxas, "Gibbs prior models, marching cubes, and deformable models: A hybrid framework for 3D medical image segmentation," *MICCAI 2003 proceedings, LNCS*, vol. 2879, pp. 703–710, 2003.
- [11] D. L. Chopp, "Computing minimal surfaces via level set curvature flow," *J. of Computational Physics*, vol. 106, no. 1, pp. 77–91, May 1993.
- [12] C. Cocosco, V. Kollokian, R. Kwan, and A. Evans, "Brainweb: Online interface to a 3D MRI simulated brain database," *NeuroImage*, vol.5, no.4, part 2/4, S425 in Proceedings of 3rd International Conference on Functional Mapping of the Human Brain, May 1997, copenhagen, <http://www.bic.mni.mcgill.ca/brainweb/>.
- [13] L. D. Cohen, "On active contour models and balloons," *CVGIP: Image understanding*, vol. 53, no. 2, pp. 211–218, 1991.
- [14] L. D. Cohen and R. Kimmel, "Global minimum for active contours models: A minimal path approach," *Int. Journal of Comp. Vis.*, vol. 24, no. 1, pp. 57–78, 1997.
- [15] M. de Bruijne, B. van Ginneken, L. Bartles, M. van der Laan, J. D. Blankensteijn, W. J. Neissen, and M. Veirgever, "Automated segmentation of abdominal aortic aneurysms in multi-spectral MR images," *MICCAI 2003 proceedings, LNCS*, vol. 2879, pp. 538–545, 2003.
- [16] T. Deschamps, "Curve and shape extraction with minimal path and level sets techniques. applications to 3D medical imaging," Ph.D. dissertation, University of Paris Daphine, 2001.
- [17] T. Deschamps and L. Cohen, "Fast extraction of tubular and tree 3D surfaces with front propagation methods," *Int. Conf. on Pat. Rec.*, vol. 1, pp. 731–734, August 2002.
- [18] Y. Fridman, S. M. Pizer, S. Aylward, and E. Bullitt, "Segmenting 3D branching tubular structures using cores," *MICCAI 2003*

- proceedings, LNCS*, vol. 2879, pp. 570–577, 2003.
- [19] D. Gering, “Diagonalized nearest neighbor pattern matching for brain tumor segmentation,” *MICCAI 2003 proceedings, LNCS*, vol. 2879, pp. 670–677, 2003.
- [20] A. Gersho and R. M. Gray, *Vector quantization and signal compression*. Kluwer, 1992, ch. 12, pp. 410–421.
- [21] R. Goldenberg, R. Kimmel, E. Rivlin, and M. Rudsky, “Fast geodesic active contours,” *IEEE Trans. Image Processing*, vol. 10(10), pp. 1467–1475, 2001.
- [22] —, “Cortex segmentation - a fast variational geometric approach,” *IEEE Trans. Med. Imag.*, vol. 21, no. 2, pp. 1544–1551, 2002.
- [23] R. Gonzales and R. Woods, *Digital Image Processing*. Addison-Wesley Publishing Company, 1992.
- [24] R. Haralik, “Digital step edges from zero crossing of second directional derivatives,” *IEEE Trans. Pattern Anal. Machine Intell.*, vol. 6(1), pp. 58–68, January 1984.
- [25] M. S. Hassouna, A. Farag, S. Hushek, and T. Moriarty, “Statistical based approach for extracting 3D blood vessels from TOF-Myra data,” *MICCAI 2003 proceedings, LNCS*, vol. 2878, pp. 680–687, 2003.
- [26] M. Hernandez, A. Frangi, and G. Sapiro, “Three dimensional segmentation of brain aneurysms in CTA using non-parametric region-based information and implicit deformable models: method and evaluation,” *MICCAI 2003 proceedings, LNCS*, vol. 2879, pp. 594–602, 2003.
- [27] M. Kass, A. Witkin, and D. Terzopolous, “Snakes: Active contour models,” *Int. Journal of Comp. Vis.*, vol. 1, no. 4, pp. 321–331, 1988.
- [28] R. Kimmel, “Fast edge integration,” in *Geometric Level Set Methods in Imaging, Vision and Graphics*, S. Osher and N. Paragios, Eds. Springer Verlag, 2003.
- [29] —, *Numerical Geometry of Images: Theory, Algorithms, and Applications*. Springer Verlag, 2003.
- [30] R. Kimmel and A. Bruckstein, “Regularized Laplacian zero crossings as optimal edge integrators,” *Proc. of Image and Vision Computing, IVCNZ01*, November 2001.
- [31] —, “On edge detection edge integration and geometric active contours,” *Int. Symp. on Math. Morph.*, pp. 37–45, April 2002.
- [32] —, “Regularized Laplacian zero crossings as optimal edge integrators,” *Int. Journal of Comp. Vis.*, vol. 53, no. 3, pp. 225–243, 2003.
- [33] M. E. Leventon, W. E. L. Grimson, and O. Faugeras, “Statistical shape influence in geodesic active contours,” in *Proc. of Computer Vision and Pattern Recognition*, pp. 1316–1323, June 2000.
- [34] S. P. Lloyd, “Least squares quantization in PCM,” *Unpublished Bell Laboratories Technical Note*, 1957, portions presented at the Institute of Mathematical Statistics Meeting Atlantic City New Jersey September 1957. Published in special issue on quantization, *IEEE Trans. Inform. Theory*, vol. 28, pp. 129–137, Mar. 1982.
- [35] L. Lorigo, O. Faugeras, W. Grimson, R. Keriven, R. Kikinis, C. Westin, and A. Nabavi, “Codimension-two geodesic active contours for the segmentation of tubular structures,” in *Proc. of Computer Vision and Pattern Recognition*, pp. 1444–1451, 2000.
- [36] T. Lu, P. Neittaanmaki, and X.-C. Tai, “A parallel splitting up method and its application for Navier-Stokes equations,” *Applied Mathematics Letters*, vol. 4, no. 2, pp. 25–29, 1991.
- [37] —, “A parallel splitting up method and for partial differential equations and its application to Navier-Stokes equations,” *RAIRO Math. Model. and Numer. Anal.*, vol. 26, no. 6, pp. 673–708, 1992.
- [38] R. Malladi, J. Sethian, and B. Vermuri, “Shape modelling with front propagation: A level set approach,” *IEEE Trans. Pattern Anal. Machine Intell.*, vol. 17, no. 2, pp. 158–175, Feb. 1995.
- [39] G. Marchuk, *Handbook of Numerical Analysis*. Amsterdam: North Holland, 1990, vol. I, ch. Splitting and Alternating Direction Methods, pp. 198–461.
- [40] D. Marr and E. Hildreth, “Theory of edge detection,” *Proc. of the Royal Society London B*, vol. 207, pp. 187–217, 1980.
- [41] T. McInerney and H. Dehmshki, “User defined B-spline template snakes,” *MICCAI 2003 proceedings, LNCS*, vol. 2879, pp. 746–753, 2003.
- [42] T. McInerney and D. Terzopoulos, “T snakes: Topology adaptive snakes,” *Medical Image Analysis 4*, pp. 73–91, 1999.
- [43] —, “Topology adaptive deformable surfaces for medical image volume segmentation,” *IEEE Trans. Med. Imag.*, vol. 18, no. 10, pp. 840–850, October 1999.
- [44] D. Mumford and J. Shah, “Optimal approximation by piecewise smooth functions and associated variational problems,” *Comm. Pure Applied Math*, vol. 42, pp. 577–685, 1989.
- [45] K. Museth, D. Breen, L. Zhukov, and R. Whitaker, “Level set segmentation from multiple non-uniform volume datasets,” *Proceedings of IEEE Visualization 2002*, pp. pp. 179–186, October 2002.
- [46] S. Osher and J. A. Sethian, “Fronts propagating with curvature dependent speed: Algorithms based on Hamilton Jacobi formulations,” *Journal of Com. Phys.*, vol. 79, pp. 12–49, 1988.
- [47] N. Paragios, “User aided boundary delineation through the propagation of implicit representation,” *MICCAI 2003 proceedings, LNCS*, vol. 2879, pp. 678–686, 2003.
- [48] D. Peng, B. Merriman, S. Osher, H.-K. Zhao, and M. Kang, “A pde-based fast local level set method,” *Journal of Com. Phys.*, vol. 155, pp. 410–438, 1999.
- [49] J. A. Sethian, *Level Set Methods: evolving interfaces in geometry, fluid mechanics, computer vision, and materials science*. Cambridge: Cambridge University Press, 1996.
- [50] J. Sethian, “A fast marching level set method for monotonically advancing fronts,” *Proc. Nat. Acad. Sci.*, vol. 93, no. 4, pp. 1591–1595, 1996.
- [51] A. Tsai, A. Yezzi, and A. Willsky, “Curve evolution implementation of the Mumford Shah functional for image segmentation, denoising, interpolation and magnification,” *IEEE Trans. Image Processing*, vol. 10, no. 8, pp. 1169–1186, 2001.
- [52] J. N. Tsitsiklis, “Efficient algorithms for globally optimal trajectories,” *IEEE Trans. on Automatic Control*, vol. 40, no. 9, pp. 1528–1538, 1995.
- [53] A. Vasilevskiy and K. Siddiqi, “Flux maximizing geometric flows,” *IEEE Trans. Pattern Anal. Machine Intell.*, vol. 24, no. 12, pp. 1565–1578, December 2002.
- [54] J. Weickert, B. ter Haar Romeny, and M. Viergever, “Efficient and reliable scheme for nonlinear diffusion filtering,” *IEEE Trans. Image Processing*, vol. 7(3), pp. 398–410, 1998.
- [55] S. Zhu and A. Yuille, “Region competition: Unifying snakes, region growing, energy/Bayes/MDL for multi-band image segmentation,” *IEEE Trans. Pattern Anal. Machine Intell.*, vol. 19, no. 9, pp. 884–900, 1996.

PLACE
PHOTO
HERE

Michal Holtzman Gazit Michal Holtzman Gazit was born in Kiriat Motzkin, Israel in 1974. She received her B.Sc in Electrical Engineering (with Honors) in 1998 and her M.Sc. in Electrical engineering in 2004, from the Technion – Israel Institute of Technology. During the years 1996-2001 she worked in Zoran Microelectronics Ltd. as an algorithm developer for imaging products. Her research interests in image processing and analysis, medical image processing and analysis, real time systems and computer vision. She presented her research results in the MICCAI conference in Montreal, Canada in 2003. She is currently pursuing her PhD in the faculty of Computer Science in the Technion – Israel Institute of Technology.

Nathan Peled Dr. Nathan Peled is the head of the Department of Radiology in the Lady Davis Carmel Medical Center, Haifa, Israel. His special interests are in pediatric radiology, computerized tomography, neuroradiology, and cardiac CT.

Ron Kimmel Ron Kimmel received his B.Sc. (with honors) in computer engineering in 1986, the M.Sc. in 1993 in electrical engineering, and the D.Sc. degree in 1995 from the Technion – Israel Institute of Technology. During the years 1986-1991 he served as an R&D officer in the Israeli Air Force.

He has been a postdoctoral fellow at Berkeley Labs, and the Mathematics Department, at UC Berkeley during 1995-1998. Since 1998, he has been a faculty member of the Computer Science Department at the Technion, where he is currently an associate professor. He spent his recent sabbatical 2003-2004 as a visiting Professor at Stanford University and working with MediGuide (biomedical imaging).

His research interests are in computational methods and their applications in: applied differential geometry, numerical analysis, image processing and analysis, robotics, and computer graphics. Prof. Kimmel was awarded the Rich innovation award (twice), the Taub Prize for excellence in research, and the Alon, HTI, Wolf, Gutwirth, Ollendorff, and Jury fellowships.

He has been a consultant of HP research Lab during 1998-2000, to Net2Wireless/Jigami research during 2000-2001, and is on the advisory board of MediGuide since 2002. He has been on various program and organizing committees of conferences, workshops, and editorial boards of image processing and analysis journals. Prof. Kimmel is the author of 'Numerical Geometry of Images' published by Springer, 2003.

Dorith Goldsher Dorith Goldsher graduated from the Faculty of Medicine at the Technion – Israel Institute of Technology in 1976 and completed her internship in 1978. She obtained Israel Board Certification in Radiology in 1983, following 5 years of Residency in the Department of Diagnostic Radiology at Rambam Medical Center in Haifa and became a Senior Radiologist. Three years later, she was granted tenure.

She was a Fellow in Neuroradiology and MRI at the Department of Radiology of New York University Hospital during 1988-9. She then returned to Rambam Medical Center and, in 1992, founded the MRI Institute, first serving as Acting Director and, since 1995, as Director.

From 1997 to 1999, she was appointed as Acting Director of the Neuroradiology Unit at Rambam Medical Center and, in 1999, as Director.

Dorith Goldsher was nominated as Chairman of Israel Society of Neuroradiology in 2002.

She was appointed as a Lecturer in the Faculty of Medicine, Technion – Israel Institute of Technology in Haifa in 1996 and Senior Lecturer in 2004.